Journal of The Electrochemical Society, **162** (10) A1990-A1996 (2015)
0013-4651/2015/162(10)/A1990/7/$33.00

Reversible Capacity Enhancement of Zinc-Manganese Mixed Oxide through Nanoscale Electrochemical Wiring with Carbon Nanotubes

Seung-Beom Yoon,[a] Suk-Woo Lee,[a] Chang-Wook Lee,[a] Sang-Hoon Park,[a] Hyun-Kyung Kim,[a] Kyung-Wan Nam,[b] Kyung-Yoon Chung,[c,*] Kwang Chul Roh,[d,z] and Kwang-Bum Kim[a,z]

[a]*Department of Materials Science and Engineering, Yonsei University, Seodaemoon-gu, Seoul 120-749, Korea*
[b]*Department of Energy and Materials Engineering, Dongguk University, Seoul, 100-715, Korea*
[c]*Center for Energy Convergence, Korea Institute of Science and Technology, Seongbuk-gu, Seoul, 136-791, Korea*
[d]*Energy Efficient Materials Team, Energy & Environmental Division, Korea Institute of Ceramic Engineering and Technology, Jinju-si, Gyeongsangnam-do, 660-031, Korea*

Zinc-manganese mixed oxide (ZMO)/carbon nanotube (CNT) composites are synthesized based on an electronic wiring design for use in Li-ion batteries. The resulting composite consists of ZMO nanoparticles in intimate contact with CNT. The ZMO nanoparticles, which are in the electrical wiring with the CNTs, exhibit an additional conversion reaction involving MnO/Mn_3O_4, resulting in an enhanced reversible capacity up to 1050 mA h g^{-1}, which exceeds the theoretical reversible capacity of $ZnMn_2O_4$ (780 mA h g^{-1}). During the synthesis of the ZMO/CNT composite, calcination in the presence of NH_3 gas not only inhibits the oxidative decomposition of the CNTs but also reduces the oxidation state of Mn in the resulting composite. The elimination of superfluous oxygen (decrease in oxidation state of Mn in ZMO) leads to a decrease in irreversible capacities during the first cycle, directly related to energy efficiency.

Manuscript submitted April 21, 2015; revised manuscript received June 16, 2015. Published July 22, 2015.

Transition metal oxides (TMOs) have been studied as anode materials for Li-ion batteries (LIBs) since Tarascon et al. first reported the reversible reactions of TMOs with Li.[1] Devices based on TMOs composed of Co, Ni, Cu, Fe, Mn, or Zn are capable of storing electrochemical energy via a reversible conversion reaction.[1–3] Although this conversion reaction could accommodate a large amount of Li atoms, voltage hysteresis is observed during charge–discharge due to the poor kinetic properties of conversion reactions. In addition, the low initial efficiency and poor cyclic performance hinders practical applications.[4,5] Thus, additional research is required to overcome these problems.

Among the various TMOs, zinc oxide (ZnO) and manganese-based oxides (MnO, Mn_3O_4, Mn_2O_3, and MnO_2) have been extensively investigated owing to their inexpensive and non-toxic constituents.[6] Pure ZnO and Mn_xO_y, however, suffer from severe capacity fading during cycling. These drawbacks arise from the pulverization of pure ZnO and Mn_xO_y due to large volume changes and the gradual agglomeration of electrochemically inactive metallic grains during repeated conversion reactions.[7–9] Therefore, significant efforts have been made toward reducing the size of the TMO particles to improve their cycling stability.[9–12]

Interestingly, $ZnMn_2O_4$, which is a combination of ZnO and Mn_2O_3, exhibits superior cycling stability regardless of the particle size compared to pure ZnO and Mn_xO_y.[3,6,13,14] The overall electrochemical reaction of $ZnMn_2O_4$ with Li consists of four electrochemical reactions, which are shown below (Eqs. 1–4).[3,6]

An irreversible reaction occurs during the first discharge (1008 mA h g^{-1}):[6]

$$ZnMn_2O_4 + 9Li^+ + 9e^- \rightarrow LiZn + 2Mn + 4Li_2O \quad [1]$$

Reversible alloying/dealloying and conversion reaction (784 mA h g^{-1}):[6]

$$Zn + Li^+ + e^- \leftrightarrow LiZn\ (\sim 0.2 \text{ and } \sim 0.7\ V \text{ vs. } Li/Li^+\text{: Oxidation}) \quad [2]$$

$$ZnO + 2Li^+ + 2e^- \leftrightarrow Zn + Li_2O\ (\sim 1.5\ V \text{ vs. } Li/Li^+\text{: Oxidation}) \quad [3]$$

$$MnO + 2Li^+ + 2e^- \leftrightarrow Mn + Li_2O\ (\sim 1.2\ V \text{ vs. } Li/Li^+\text{: Oxidation}) \quad [4]$$

As shown in Eqs. 1–4, $ZnMn_2O_4$ intrinsically has an irreversible capacity ascribed to the oxidation state of Mn during the first discharge. While the oxidation number of Mn in $ZnMn_2O_4$ is +3, it changes only between 0 (Mn^0) and +2 (Mn^{2+}) during the reversible electrochemical reactions in $ZnMn_2O_4$. Moreover, considering the additional irreversibility due to the formation of solid electrolyte interface (SEI) films on the particle surfaces, reducing the irreversible capacities during the first cycle seems to be crucial for adopting $ZnMn_2O_4$ as anode materials for LIB applications. As with pure ZnO and Mn_xO_y, recent studies on $ZnMn_2O_4$ have focused on controlling the particle size and morphology at the nanometer scale to further improve its electrochemical properties. However, those efforts do not appear to improve the reversible specific capacity of $ZnMn_2O_4$. Most electrochemical studies on $ZnMn_2O_4$ have reported large irreversible capacities during the first cycle despite its novel morphology.[3,6,13,15–22]

As aforementioned, one primary reason for the irreversibility of $ZnMn_2O_4$ during the first cycle is the oxidation state of Mn. Therefore, increasing the reversible capacity of the Mn species in $ZnMn_2O_4$ is one of the most effective solutions for reducing irreversibility during the first cycle. In a recent study of $ZnMn_2O_4$, an additional reversible conversion reaction involving Mn has been suggested:[13]

$$2/3\,Mn_3O_4 + 4/3\,Li^+ + 4/3\,e^- \leftrightarrow 2\,MnO + 2/3\,Li_2O \quad [5]$$

Although the reversible conversion reaction of Mn-based oxides has been considered an electrochemical reaction between MnO and Mn (Eq. 4),[23,24] the reversible conversion between Mn_3O_4 and MnO (Eq. 5) has been observed in several reports on MnO_x composites containing a large amount of electrically conductive agents.[11,25–27] This suggests that the reversible conversion of Mn_3O_4/MnO is a thermodynamically favorable reaction, but it is affected by the electrochemical kinetic properties of the reaction. If the electrochemical kinetics of the conversion reaction are improved, not only specific capacity but also the initial coulombic efficiency can be improved.

Herein, we report the synthesis of Zn-Mn mixed oxide (ZMO)/carbon nanotube (CNT) composites. The kinetic properties of the electrochemical reaction are influenced by the electrochemical wiring topology.[28,29] We demonstrate that the reversible capacity of the mixed oxide can be enhanced through nanoscale electrochemical wiring using CNTs. In order to investigate the effect of electrochemical wiring on the kinetics of the reversible conversion reactions in the system, the electrochemical properties of the ZMO/CNT composite have been compared to those of $ZnMn_2O_4$ particles with poor electronic wiring.

*Electrochemical Society Active Member.
[z]E-mail: rkc@kicet.re.kr; kbkim@yonsei.ac.kr

Experimental

Preparation of ZMO/CNT composites.— The ZMO/CNT composite was fabricated by the calcination of a mixture of $Zn(OH)_2$ with a MnO_2/CNT composite. The MnO_2/CNT composite was synthesized by a direct redox reaction between the CNTs and permanganate ions in an aqueous solution; the detailed procedure is described elsewhere.[30] To fabricate the ZMO/CNT composite, $Zn(NO_3)_2$ (0.37 g) and MnO_2/CNT (0.34 g) were homogeneously dispersed in 200 mL of deionized (DI) water using a horn-type sonicator. An aqueous solution of NH_4OH (25 vol.%; 1.5 mL) was added to the suspension dropwise with constant mechanical stirring (feed rate: 0.7 mL h^{-1}). As the pH of the dispersion increased, $Zn(OH)_2$ was precipitated. After 8 h, the resulting suspension was filtered, and the residue was repeatedly washed with DI water and ethanol. Finally, the mixture was calcined at 500°C using NH_3 (1 vol.%) and O_2 (1 vol.%) in an Ar gas stream. For comparison, $ZnMn_2O_4$ particles were synthesized by calcination of the same mixture at 500°C in air. Since the NH_3 gas is toxic, the calcination is conducted in the fume hood with a ventilation system.

Characterization of the ZMO/CNT composite.— Transmission electron microscopy (TEM) and energy-dispersive X-ray spectroscopic (EDS) analyses were performed using a field-emission transmission electron microscope (FE-TEM; JEM-2100F, JEOL Ltd.). The morphology of the composite was characterized by scanning electron microscopy (SEM; S-4300SE, Hitachi High-Technologies Co.). The crystallinity of the composite was determined by X-ray diffraction (XRD; Rigaku, Cu Kα, 40 kV, 20 mA). The ZMO loading in the composites was determined by thermogravimetric analysis (TGA; STA 409 PC, NETZSCH-Gerätebau GmbH), which was conducted under air flow at a temperature ramp rate of 10°C min^{-1} from room temperature to 800°C. The chemical states of the ZMO phases were determined using X-ray photoelectron spectroscopy (XPS; PHI 5000 VersaProbe ULVAC-PHI, Inc.) with Al Kα radiation (1486.6 eV). The binding energy peaks were corrected for specimen charging by referencing the C 1s peak at 284.6 eV. The Raman spectrum of the composite was measured to characterize the ZMO structure using a Jobin Yvon LabRam HR (HORIBA, Ltd.) with a liquid N_2-cooled charge-coupled device (CCD) multichannel detector at room temperature. Conventional backscattering geometry was used, and a 514.5-nm Ar-ion laser was used as the light source. The peaks are fitted using a mixture of Gaussian (90%) and Lorentzian (10%) functions. The Mn K-edge X-ray absorption spectra (XAS) were measured in transmission mode at the 1D-XRS KIST-PAL (XAFS) beamline of the Pohang Light Source (PLS) using a Si(1 1 1) double-crystal monochromator. Calibration of Mn K-edge energy was performed using the first inflection point of the spectrum of Mn metal foil as a reference (i.e., Mn K-edge = 6539 eV). The reference spectra were collected simultaneously for each spectrum using a Mn metal foil.

Electrochemical measurements of the ZMO/CNT composite.— The electrochemical properties of the ZMO/CNT composite were investigated using 2032 coin cells, with lithium foil as the counter electrode and 1.3 M $LiPF_6$ in a mixture of ethyl carbonate (EC), diethyl carbonate (DEC), and fluoroethylene carbonate (*FEC*) (2:6:2 v/v/v) as the electrolyte. There have been reports of positive effects of fluoroethylene carbonate (FEC) as a co-solvent in alkyl carbonate on the stability of anode materials with high volume changes during cycling.[31] The working electrode was prepared by slurry casting a mixture of 90 wt% ZMO/CNT and 10 wt% poly(3,4-ethylenedioxythiophene)poly(styrene sulfonate) (PEDOT:PSS) binder onto a Cu foil. For comparison, we also prepared a $ZnMn_2O_4$ electrode composed of $ZnMn_2O_4$ particles, various amounts of acetylene black (AB), and 10 wt% PEDOT:PSS. The weight of the active materials in the electrode was controlled at approximately 2.6 mg cm^{-2}. The electrochemical characterization experiments were performed in the potential range of 3.0–0.001 V using a potentiostat/galvanostat (VMP3, Bio-Logic). The specific capacity of the ZMO/CNT composite was calculated based on weight, whereas that of the $ZnMn_2O_4$ particles was calculated based on the weight of $ZnMn_2O_4$ alone, excluding the weight of AB.

Results and Discussion

A Zn-Mn precursor should be calcined under air containing O_2 to obtain ZMO particles, with a Mn oxidation number of +2.6. On the other hand, ZnO and MnO are synthesized by calcination under Ar atmosphere.[32] However, CNTs need to be protected from oxidative decomposition in order to synthesize the CNT composite. Therefore, an NH_3/O_2 gas mixture was employed for the ZMO/CNT composite synthesis to overcome this limitation. The $Zn(OH)_2$-MnO_2/CNT mixture was calcined under an NH_3/O_2 gaseous mixture in Ar. Gaseous NH_3 inhibits the oxidative decomposition of the CNTs by sacrificial oxidization. Wang et al. reported that the addition of NH_3 to O_2 in Ar considerably decreases the rate of graphene etching by oxidative decomposition.[33] For comparison, $ZnMn_2O_4$ particles were prepared by calcination of the same precursor under air.

In order to improve the electronic wiring in the composite, large numbers of ZMO particles are required to be in contact with electrically conductive materials. Therefore, the MnO_2/CNT composite was used as a precursor for fabricating the ZMO/CNT composite. As mentioned previously, $Zn(OH)_2$ was precipitated in the MnO_2/CNT dispersion by controlling the pH of the dispersion. After calcination, the layer morphology of $Zn(OH)_2$-MnO_2 on CNT transitions to a particle morphology as a result of formation of ZMO particles. Sample morphologies as a function of calcination conditions are shown in Figure 1. The TEM and SEM images of the ZMO/CNT composite revealed uniformly dispersed $ZnMn_2O_4$ particles on the CNTs (Figures 1a, 1c). In the case of calcination in air, the $ZnMn_2O_4$ particles were linearly linked, even though the CNTs were decomposed (Figures 1b, 1d). The particle sizes of ZMO (~15 nm) in the CNT composite were comparable to those of pristine $ZnMn_2O_4$, as determined by TEM.

The XRD patterns of the ZMO/CNT composite and $ZnMn_2O_4$ particles are shown in Figure 2. The ZMO/CNT composite and $ZnMn_2O_4$ particles exhibited broad peaks due to the low calcination temperature, indicating that the prepared samples have poor crystallinity. Peaks ascribed to the spinel structure of the prepared TMO were observed in the XRD patterns of both materials, and small peaks originating

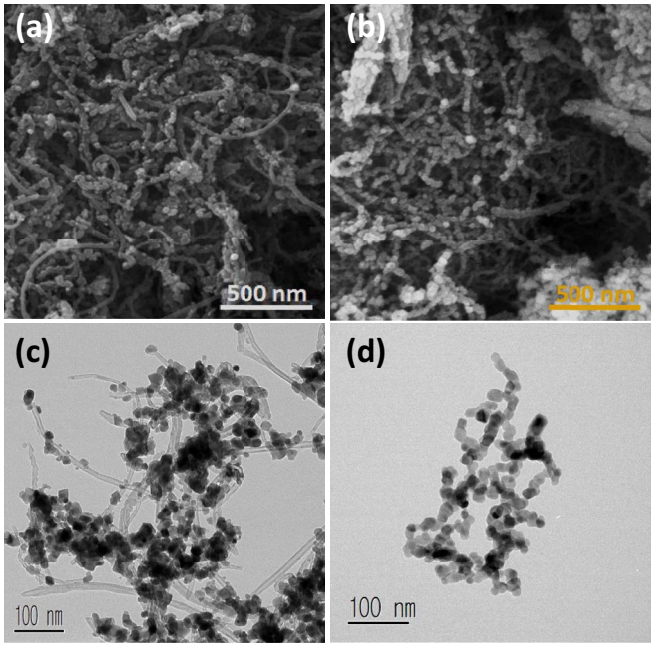

Figure 1. The TEM and SEM images of the (a, c) ZMO/CNT composite and (b, d) $ZnMn_2O_4$ particles.

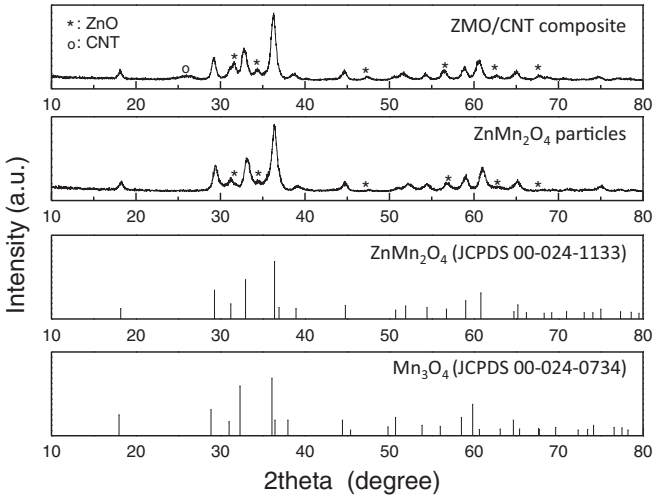

Figure 2. The XRD patterns of the ZMO/CNT composite and $ZnMn_2O_4$ particles.

from ZnO were observed at 2θ values of 31.6, 34.4, 47.5, 56.5, 62.9, and 67.8°. An additional broad peak attributed to the CNTs was observed only in the ZMO/CNT composite. It is noteworthy that the 2θ values of the peaks ascribed to the ZMO/CNT composite were slightly lower than those of the $ZnMn_2O_4$ particles, indicating a structural difference between the ZMO/CNT composite and the $ZnMn_2O_4$ particles. Generally, $ZnMn_2O_4$ has a spinel structure in which the tetrahedral and octahedral sites are occupied by Zn^{2+} and Mn^{3+}, respectively. The 2θ values corresponding to spinel Mn_3O_4 are lower than those of $ZnMn_2O_4$, despite their isostructural similarities. The difference in the peak positions between the ZMO/CNT composite and the $ZnMn_2O_4$ particles may be ascribed to the presence of Mn_3O_4 in the prepared ZMO/CNT composite. The ZMO/CNT composite also showed an increased peak intensity ratio compared to the $ZnMn_2O_4$ particles, which may be ascribed to the presence of ZnO. It is difficult to directly compare the characteristics of compounds based on the intensities of the peaks in the XRD patterns; however, based on the intensity ratio of ZnO to $ZnMn_2O_4$, it is reasonable to suggest that the ZMO/CNT composite likely contains a larger amount of ZnO than $ZnMn_2O_4$ particles. This suggests that Zn^{2+} ions were unable to move into the tetrahedral sites during calcination, which might result in the formation of Mn_3O_4 in the ZMO/CNT composite.

Because the prepared samples have poor crystallinity, conclusions on the presence of Mn_3O_4 in the ZMO/CNT composite using only XRD data might be speculative. Therefore, the oxidation numbers and band properties of Mn and Zn were characterized through XPS analyses. The XPS spectra of the ZMO/CNT composite and $ZnMn_2O_4$ particles are shown in Figure 3. The Mn $2p_{3/2}$ peak could be deconvoluted into Mn^{2+} and Mn^{3+} bands.[34] As shown in Figure 3a, the area of the Mn^{2+} band in the XPS spectrum for the ZMO/CNT composite is larger than the corresponding value for the $ZnMn_2O_4$ particles, indicating that Mn^{2+} partially replaces Zn^{2+} in the tetrahedral sites of the spinel structure. While pure ZnO exhibits a symmetric Zn $2p_{3/2}$ peak in its spectrum, the Zn and Mn hybrid oxide exhibits an asymmetric Zn $2p_{3/2}$ peak that can be deconvoluted into the Zn-O and Zn-Mn bands.[34] The area of the Zn-O band in the XPS spectrum of the ZMO/CNT composite is larger than that of the $ZnMn_2O_4$ particles (Figure 3b). Since NH_3 is a strong reducing agent, it is expected to partially reduce the Mn_2O_3 in $ZnMn_2O_4$ to Mn_3O_4, as well as protect the CNTs from oxidative decomposition during calcination. The reductive conditions due to the presence of NH_3 inhibit the incorporation of Zn into the spinel Mn_3O_4 structure and induce partial phase segregation of pure ZnO and Mn_3O_4. The Raman spectrum of the ZMO/CNT composite, which is shown in Figure S5, also suggests partial phase segregation. The XRD, XPS, and Raman spectral analyses indicate that the oxidation number of Mn in the ZMO/CNT composite is less than

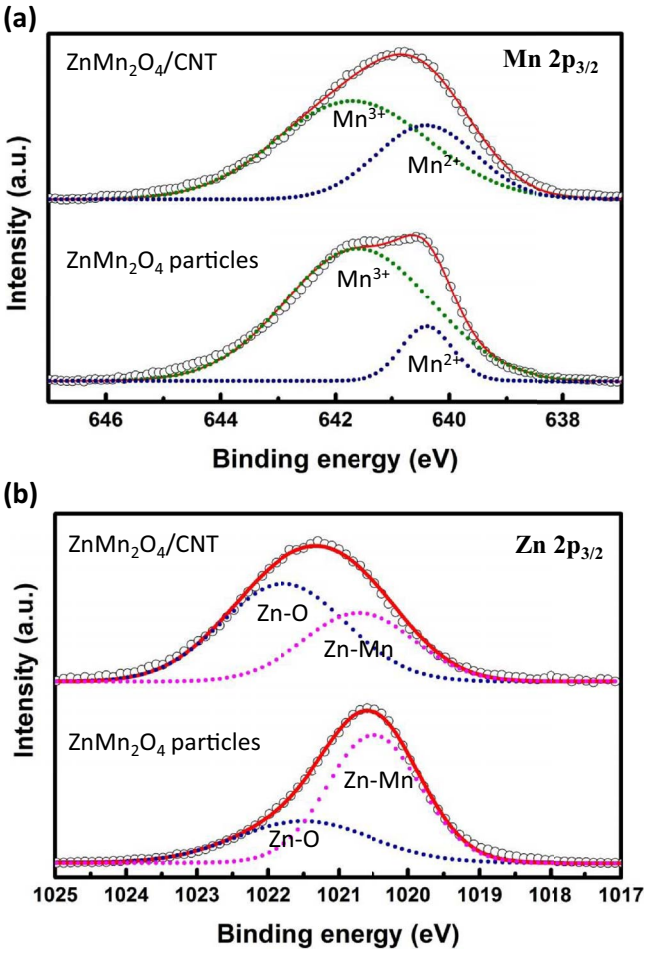

Figure 3. The XPS spectra of the ZMO/CNT composite and $ZnMn_2O_4$ particles: (a) Mn $2p_{3/2}$ and (b) Zn $2p_{3/2}$.

+3. Therefore, the irreversible capacity caused by the high oxidation number of Mn is expected to be reduced in the ZMO/composite.

To evaluate the electrochemical properties of the ZMO/CNT composite and $ZnMn_2O_4$ particles, cyclic voltammetry and galvanostatic charge–discharge tests were conducted. The ZMO content in the ZMO/CNT composite was determined to be 82% by TGA (Figure S4). When the ZMO/CNT composite electrode is fabricated, the ZMO/CNT composite electrode contained around 16 wt% carbon (ZMO/CNTs/binder = 74:16:10). In order to exclude the effect of the carbon content on the electrical conductivity of the electrode, AB (20 wt%) was added to the $ZnMn_2O_4$ particle electrode. While the current density and specific capacity of the $ZnMn_2O_4$ particle electrodes were calculated based on the weight of $ZnMn_2O_4$ alone (excluding the weight of AB), those of the ZMO/CNT composite were calculated using the composite mass including that of the CNTs. Figure 4 shows the first three galvanostatic charge–discharge cycle profiles of the ZMO/CNT composite and $ZnMn_2O_4$ particle electrodes at a current density of 100 mA g^{-1}. As shown in Figure 4a, the discharge and charge capacities of the ZMO/CNT composite in the first cycle were about 1250 and 888 mA h g^{-1}, respectively. The initial coulombic efficiency of the ZMO/CNT composite was 71%, which is significantly higher than values previously reported for $ZnMn_2O_4$.[3,6,13,15–22] As shown in Figure 4b, the $ZnMn_2O_4$ particles containing AB exhibit low specific capacities and poor first cycle coulombic efficiencies compared to the ZMO/CNT composite. The specific capacity of the $ZnMn_2O_4$ particle electrode increases with an increase in the AB content. However, the capacities of all examined $ZnMn_2O_4$ particle electrodes were still lower than that of the ZMO/CNT composite (Figure 4c).

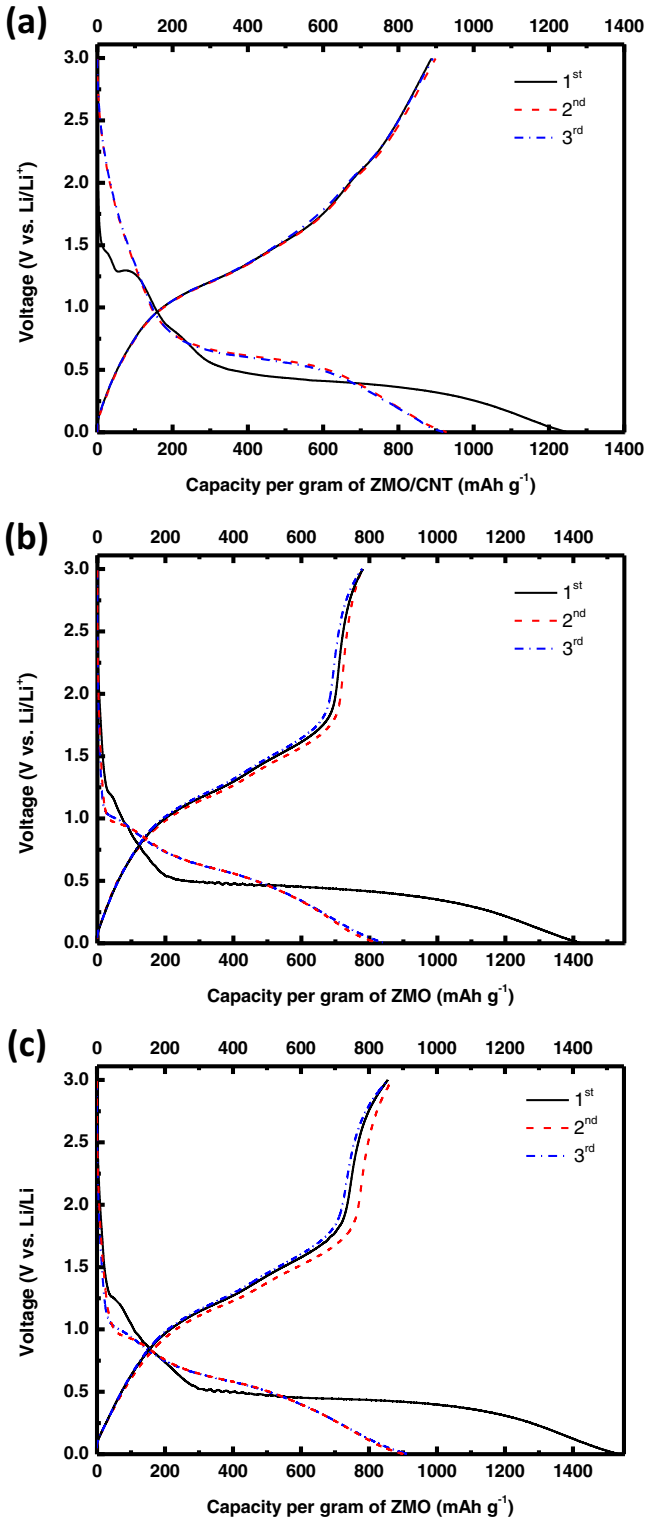

Figure 4. The first, second, and third galvanostatic charge–discharge profiles of (a) the ZMO/CNT composite and $ZnMn_2O_4$ particles with (b) 20 wt% and (c) 30 wt% AB at a current density of 100 mA g^{-1}.

Furthermore, $ZnMn_2O_4$ particle electrodes with higher AB contents still exhibited poor first cycle coulombic efficiencies compared to the ZMO/CNT composite. While the ZMO/CNT composite showed sloped discharge–charge profiles, the $ZnMn_2O_4$ particle electrodes exhibited sharp voltage drops/rises in the high voltage region. As the AB content increased, slightly sloped discharge–charge profiles were observed above 2.5 V. However, comparison of the charge–discharge

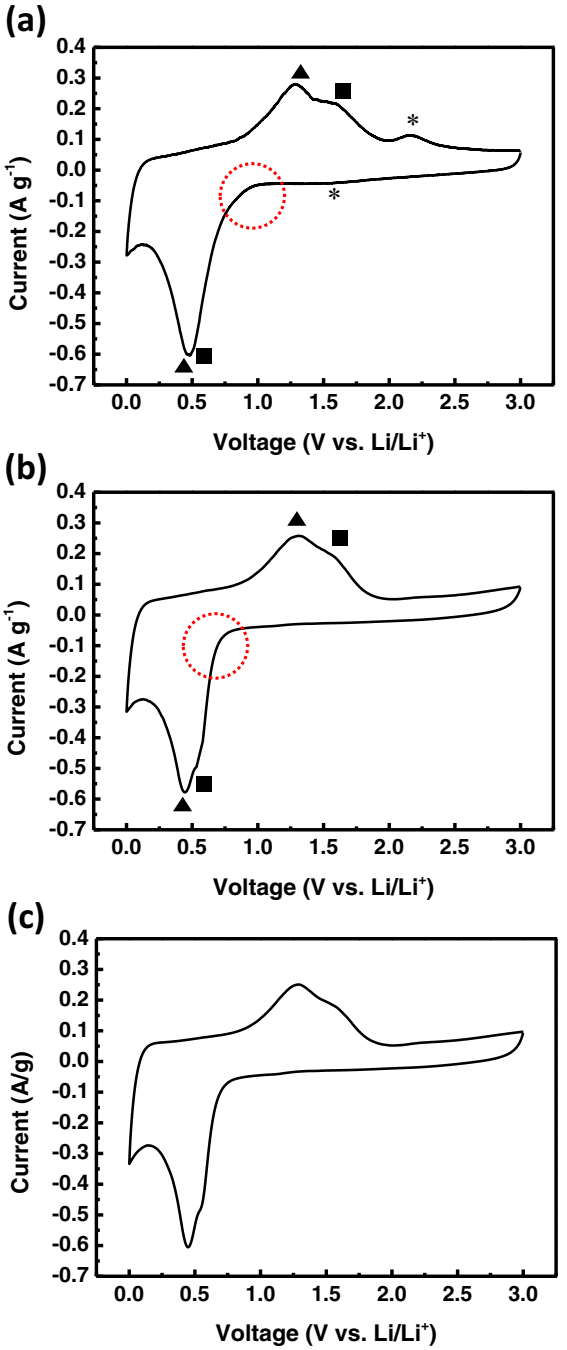

Figure 5. Cyclic voltammograms of (a) the ZMO/CNT composite and $ZnMn_2O_4$ particles with (b) 20 wt% and (c) 30 wt% AB, measured at a scan rate of 0.1 mV s^{-1}.

profiles of the ZMO/CNT composite with those of the $ZnMn_2O_4$ particles reveals clear differences in the high voltage region.

Figure 5 shows cyclic voltammograms (CV) of the ZMO/CNT composite electrode and $ZnMn_2O_4$ particle electrode containing AB, measured at a scan rate of 0.1 mV s^{-1}. According to literature, the peaks corresponding to the conversion reactions can be distinguished.[3,25,35] While only peaks related to conversion reactions involving MnO/Mn (triangles in Figure 5) and ZnO/Zn (squares in Figure 5) are observed in the CV of the $ZnMn_2O_4$ particle electrode, an additional conversion reaction peak involving MnO/Mn_3O_4 (asterisk in Figure 5) is observed in the ZMO/CNT composite. In the $ZnMn_2O_4$ particle electrode, the peak corresponding to the oxidation of MnO to Mn_3O_4 during the delithiation process was not observed

even at high AB contents, as shown in Figure 5c. It is highly probable that any overpotential associated with the electrochemical reactions may inhibit the conversion reaction when the maximum potential is limited to 3 V. It is noteworthy that both samples exhibited similar peaks at potentials corresponding to the conversion reactions involving MnO/Mn and ZnO/Zn, regardless of the presence of CNT. This indicates that both samples have similar kinetic properties for electrochemical reactions involving the metallic phase, which might be attributed to the high electrical conductivity of the metallic phase. During the lithiation process, which involves conversion from the metal oxide to the metallic phase, the ZMO/CNT composite electrode shows a higher onset potential (indicated by a red circle) than the $ZnMn_2O_4$ particle electrode, even though they exhibit similar peak potentials in the CV data. This difference in onset potential might be due to the electrochemical conversion from the poorly conducting metal oxide phase to the metal phase. While the electrode contains poorly conducting metal oxide during the initial reaction stages, the highly conducting metallic phase is produced during the reaction. Therefore, in the case that the electrochemical reaction produces the metallic phase, the peak potentials of the ZMO/CNT composite might be comparable to that of the $ZnMn_2O_4$ particles, even though the onset potentials are different.

In order to investigate the oxidation state of Mn, we conducted X-ray absorption near-edge spectroscopy (XANES) experiments. The XANES spectra revealed that the oxidation state of Mn in the as-prepared ZMO/CNT composite was different from that in $ZnMn_2O_4$ particles. The oxidation state of Mn in the ZMO/CNT composite electrode was lower than that in the $ZnMn_2O_4$ particle electrode, as shown in Figure 6. This result is consistent with the other characterization results, including XRD, XPS, and Raman spectroscopy. In order to compare the electrochemical kinetic properties, ex-situ XANES spectra were investigated to understand the oxidation state of Mn as a function of the cutoff voltage during the first delithiation process. The cutoff voltages (1.3, 1.7, 2.3, and 3.0 V vs. Li/Li^+) are chosen by considering the electrochemical potential of the Mn/MnO and MnO/Mn_3O_4 conversion reaction. Additionally, XANES spectra of the samples were obtained after constant current–constant voltage (CC-CV) charging at 3.0 V. The XANES spectra for Mn in the ZMO/CNT composite electrode acquired during the oxidation process revealed that the entire edge continuously shifted toward higher energies, as shown in Figure 6a. By increasing the cutoff voltage, the oxidation state of Mn in the ZMO/CNT composite appears to increase above that of Mn^{2+} compared to the XANES spectra of manganese oxide with various oxidation states in Figure 6c. This indicates that the electrochemical conversion reaction involving Mn_3O_4/MnO can occur below 3.0 V. Although a small increase in the oxidation state of Mn is observed in the XANES spectrum obtained after CC-CV charging at 3.0 V, the oxidation state of Mn obtained after only CC charging to 3.0 V is close to that in the as-prepared sample, suggesting that the ZMO/CNT composite has little irreversible capacity ascribed to Mn. However, the $ZnMn_2O_4$ particles exhibit poor kinetic properties for the Mn_3O_4/MnO conversion reaction. While there is little change in the oxidation state of Mn in the $ZnMn_2O_4$ particles after CC charging to 3.0 V, the oxidation state of Mn increases above that of Mn^{2+} after CC-CV charging and is close to that found in the ZMO/CNT composite. This suggests that the electrochemical reaction of Mn_3O_4/MnO is influenced by the kinetic properties, and the ZMO/CNT composite has improved electrochemical kinetics.

The electrochemical kinetic properties are closely related to electrochemical reaction sites. The electrochemical reaction sites can be classified into surface (red) and bulk (green) reaction sites, as shown in Figure 7, and the different electrochemical kinetic properties observed depend on the type of reaction site involved.[36] Electron transfer, which is directly related to the current flow, only occurs at surface reaction sites. On the other hand, bulk reaction sites are involved in charge storage through the diffusion of Li^+ ions, which are inserted into or extracted from electroactive materials following electrochemical reactions at the surface. In the electrochemical cell, the applied/measured potential is related to the concentration of oxidized and reduced species at the electrode/electrolyte interface. In general, the charge transfer rate at the surface is faster than the diffusion rate in the bulk. During current flow, a concentration difference is generated between the surface and bulk electrochemical reaction sites due to kinetic limitations ascribed to the diffusion of Li^+ ions in the solid. As a result, there is a difference between the applied/measured potential and the equilibrium potential. In other words, kinetic limitation due to the diffusion of Li^+ ions in the solid leads to overpotential.

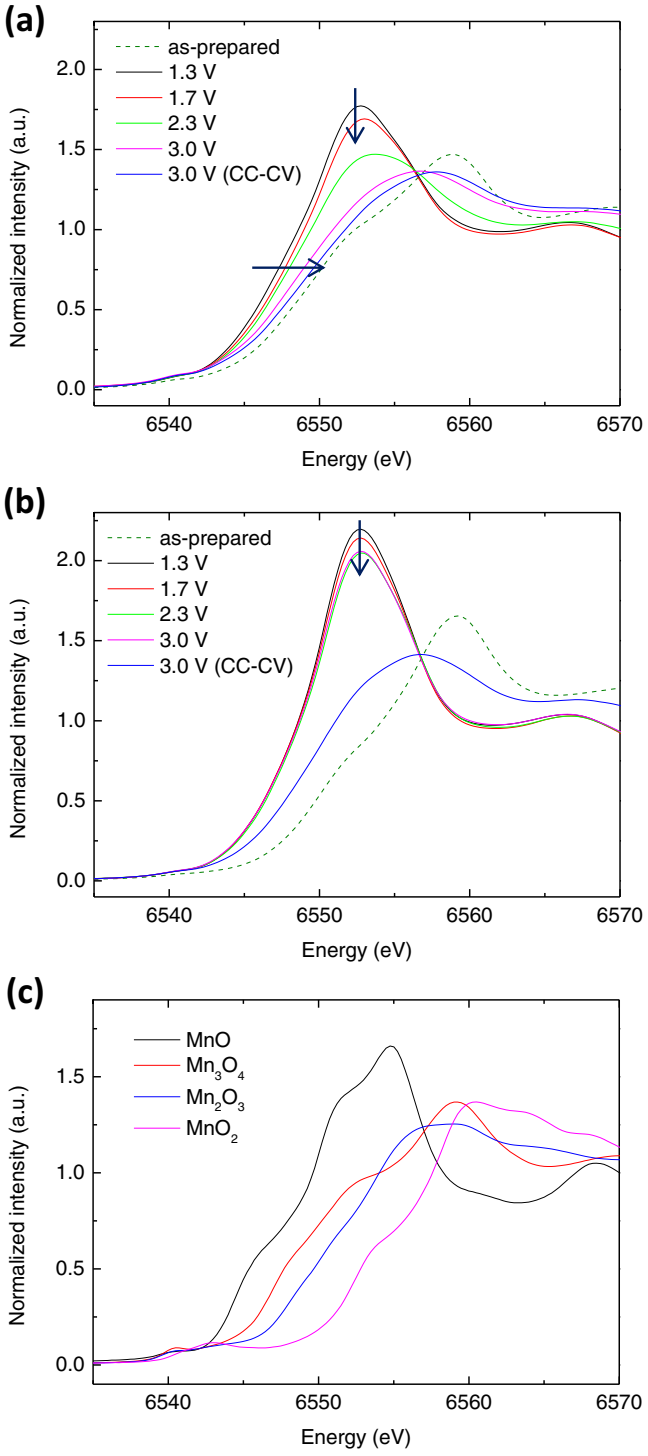

Figure 6. The XANES spectra of (a) the ZMO/CNT composite and (b) $ZnMn_2O_4$ particles at various cutoff voltages (1.3, 1.7, 2.3, and 3.0 V vs. Li/Li^+). (c) The XANES spectra of manganese oxides with various oxidation states.

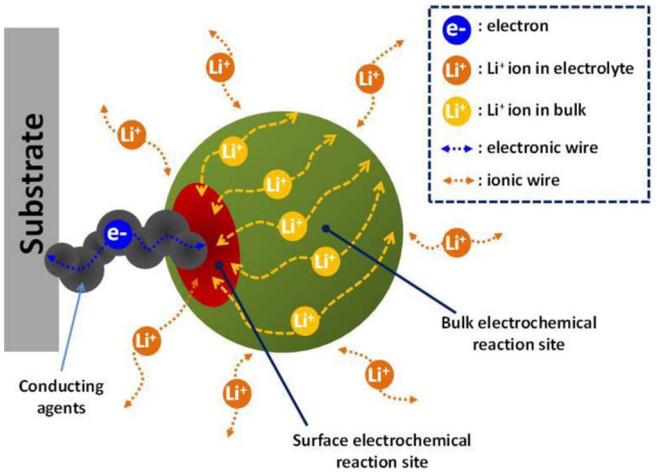

Figure 7. Schematic illustration of the relationship between the electrochemical reaction sites and electrochemical wiring.[31]

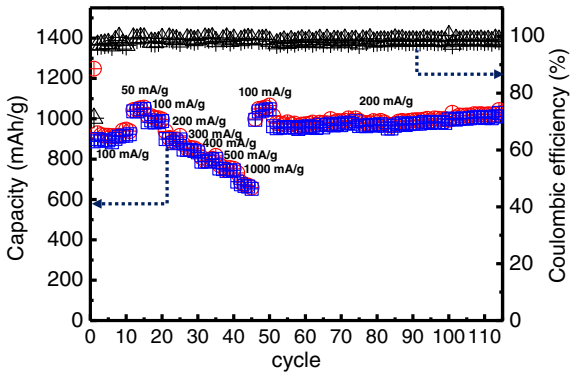

Figure 8. Results of the galvanostatic cycling tests of the $ZnMn_2O_4$/CNT composite.

Because the diffusion rate is related to the diffusion coefficient and diffusion area, these parameters should be improved to decrease these kinetic limitations. Considering that the diffusion coefficient is related to intrinsic material properties such as the lattice parameter and the interaction of the material with Li^+ ions, controlling this diffusion coefficient might be difficult. However, controlling the diffusion area could be a feasible method for improving the electrochemical kinetics.

The area of the surface electrochemical reaction sites is related to the diffusion area of bulk electrochemical reaction sites. As the number of surface electrochemical reaction sites increases, the number of bulk sites decreases.[36,37] Thus, increasing the area of surface electrochemical reaction sites is one of the most effective ways to improve the rate capability of electrode materials. While $ZnMn_2O_4$ nanoparticles have been previously synthesized, reversible electrochemical reactions involving Mn_3O_4/MnO have not been observed in these cases. In this study, the ZMO/CNT composite and $ZnMn_2O_4$ particles sizes are comparable, indicating that the morphology of the electroactive materials does not influence the electrochemical reaction sites. This suggests that compositing with CNT improves the electrochemical kinetic properties of ZMO. Thus, the composite with CNT can improve the electrical conductivity of the electrode. However, the enhanced electrical conductivity alone does not appear to improve the kinetics of the Mn_3O_4/MnO conversion reaction. Table I shows the electrical conductivities of the ZMO/CNT composite and $ZnMn_2O_4$ particle electrodes with various AB contents. Although all $ZnMn_2O_4$ particle electrodes containing AB show higher electrical conductivities than the ZMO/CNT composite electrode, the reversible Mn_3O_4/MnO reaction was not observed in $ZnMn_2O_4$ particle electrodes.

The electrochemical reaction involves several steps, such as electron supply, ion supply, electron transfer, and ion diffusion in the solid.[36,37] Because solid-state diffusion is the slowest step in the electrochemical reaction, the rate-determining step for charge storage is ion diffusion in the solid. The surface electrochemical reaction sites can be distinguished from bulk electrochemical reaction sites based on the type of electrochemical wiring such as electronic and ionic wiring, as shown in Figure 7. The electroactive material is in contact with the electrolyte (ionic wiring) and the conducting agent (electronic wiring). The surface electrochemical reaction sites are connected to both electronic and ionic wires, whereas bulk electrochemical reaction sites are not connected to either electronic or ionic wires. In our previous study, we determined that electronic wiring is a crucial factor for increasing the number of surface electrochemical reaction sites.[29] Though the fabrication of nanosized materials leads to an increase in the surface area with the decrease in the particle size, it does not cause an increase in the number of surface electrochemical reaction sites or a decrease in the number of bulk electrochemical reaction sites. The fabrication of nanomaterials only improves ionic wiring. To increase the number of surface electrochemical reaction sites, the surface of the electroactive materials must be in contact with electrically conductive materials (added to improve the electronic wiring) at the nanoscale (e.g., nanocomposite formation with nanocarbon). Therefore, the reversible Mn_3O_4/MnO redox reaction in the ZMO/CNT composite is induced by the change in surface electrochemical reaction sites, which depends on the electronic wiring topology.

Galvanostatic cycling measurements were employed to examine the electrochemical properties of the materials. As shown in Figure 8, the ZMO/CNT composite exhibits good cycling performance without capacity fading and the specific capacity increases up to 1050 mA h g^{-1}. Zheng et al. reported that the presence of impurities could cause poor capacity retention.[22] Although a minute amount of ZnO was detected as an impurity in the ZMO/CNT composite, its presence did not appear to influence the cyclability of the composite.

Considering the high surface area and short diffusion length, the synthesis of nanosized $ZnMn_2O_4$ is important for improving the electrochemical performance of LIBs. When the prepared $ZnMn_2O_4$ nanoparticles are used as electrodes, improved electrochemical performance is not always observed. Therefore, it may be concluded that the inclusion of nanoscale electrical wiring is crucial for exploiting the advantages of nanoparticles.

Table I. Electrical conductivity of the ZMO/CNT composite and $ZnMn_2O_4$ nanoparticles with different AB contents.

Sample	ZMO/CNT composites	$ZnMn_2O_4$ particles with 10 wt% AB	$ZnMn_2O_4$ particles with 20 wt% AB	$ZnMn_2O_4$ particles with 30 wt% AB
Electronic conductivity (S cm^{-1})	0.19	0.82	1.21	1.19

Conclusions

A ZMO/CNT composite, which was designed and fabricated based on an electronic wiring topology, afforded high specific capacities due to the introduction of additional capacity. The ZMO/CNT composite was synthesized by the calcination of a $Zn(OH)_2$-MnO_2/CNT mixture under an NH_3/O_2 atmosphere to prevent oxidative decomposition of the CNTs. In addition, the reductive properties ascribed to NH_3 also control the oxidation state of Mn in the resulting composite. The prepared ZMO/CNT composite with extensive electronic wiring exhibited a remarkably improved reversible capacity (1050 mA h g^{-1}) and a decrease in the irreversible capacity due to the additional conversion reaction of Mn_3O_4 to MnO.

Acknowledgments

This work was supported by Energy Efficiency & Resources program of the Korea Institute of Energy Technology Evaluation Planning (KETEP) granted financial resource from the Korea government Ministry of Trade, Industry & Energy (No. 20122010100140), by Technology Development Program for Strategic Core Materials funded by the Ministry of Trade, Industry & Energy, Republic of Korea (Project No. 10047758), and by Basic Science Research Program through the National Research Foundation of Korea (NRF) funded by the Ministry of Science, ICT & Future Planning (2015R1A2A2A03006633).

References

1. P. Poizot, S. Laruelle, S. Grugeon, L. DuPont, and J. M. Tarascon, *Nature*, **407**, 496 (2000).
2. P. Poizot, S. Laruelle, S. Grugeon, and J.-M. Tarascon, *Journal of The Electrochemical Society*, **149**, A1212 (2002).
3. F. M. Courtel, H. Duncan, Y. Abu-Lebdeh, and I. J. Davidson, *Journal of Materials Chemistry*, **21**, 10206 (2011).
4. X. W. Lou, D. Deng, J. Y. Lee, J. Feng, and L. A. Archer, *Advanced Materials*, **20**, 258 (2008).
5. G. Binotto, D. Larcher, A. S. Prakash, R. Herrera Urbina, M. S. Hegde, and J. M. Tarascon, *Chemistry of Materials*, **19**, 3032 (2007).
6. L. Xiao, Y. Yang, J. Yin, Q. Li, and L. Zhang, *Journal of Power Sources*, **194**, 1089 (2009).
7. J. Fan, T. Wang, C. Yu, B. Tu, Z. Jiang, and D. Zhao, *Advanced Materials*, **16**, 1432 (2004).
8. F. Cheng, Z. Tao, J. Liang, and J. Chen, *Chemistry of Materials*, **20**, 667 (2007).
9. J. Guo, Q. Liu, C. Wang, and M. R. Zachariah, *Advanced Functional Materials*, **22**, 803 (2012).
10. M.-S. Wu, P.-C. J. Chiang, J.-T. Lee, and J.-C. Lin, *The Journal of Physical Chemistry B*, **109**, 23279 (2005).
11. H. Wang, L.-F. Cui, Y. Yang, H. Sanchez Casalongue, J. T. Robinson, Y. Liang, Y. Cui, and H. Dai, *Journal of the American Chemical Society*, **132**, 13978 (2010).
12. X. Shen, D. Mu, S. Chen, B. Wu, and F. Wu, *ACS Applied Materials & Interfaces*, **5**, 3118 (2013).
13. S.-W. Kim, H.-W. Lee, P. Muralidharan, D.-H. Seo, W.-S. Yoon, D. Kim, and K. Kang, *Nano Research*, **4**, 505 (2011).
14. C. Yuan, H. B. Wu, Y. Xie, and X. W. Lou, *Angewandte Chemie International Edition*, **53**, 1488 (2014).
15. G. Zhang, L. Yu, H. B. Wu, H. E. Hoster, and X. W. Lou, *Advanced Materials*, **24**, 4609 (2012).
16. Z. Bai, N. Fan, C. Sun, Z. Ju, C. Guo, J. Yang, and Y. Qian, *Nanoscale*, **5**, 2442 (2013).
17. Y. Yang, Y. Zhao, L. Xiao, and L. Zhang, *Electrochemistry Communications*, **10**, 1117 (2008).
18. Y. Deng, S. Tang, Q. Zhang, Z. Shi, L. Zhang, S. Zhan, and G. Chen, *Journal of Materials Chemistry*, **21**, 11987 (2011).
19. F. M. Courtel, Y. Abu-Lebdeh, and I. J. Davidson, *Electrochimica Acta*, **71**, 123 (2012).
20. L. Zhou, H. B. Wu, T. Zhu, and X. W. Lou, *Journal of Materials Chemistry*, **22**, 827 (2012).
21. P. F. Teh, Y. Sharma, Y. W. Ko, S. S. Pramana, and M. Srinivasan, *RSC Advances*, **3**, 2812 (2013).
22. Z. Zheng, Y. Cheng, X. Yan, R. Wang, and P. Zhang, *Journal of Materials Chemistry A*, **2**, 149 (2014).
23. X. Fang, X. Lu, X. Guo, Y. Mao, Y.-S. Hu, J. Wang, Z. Wang, F. Wu, H. Liu, and L. Chen, *Electrochemistry Communications*, **12**, 1520 (2010).
24. M. A. Lowe, J. Gao, and H. D. Abruna, *Journal of Materials Chemistry A*, **1**, 2094 (2013).
25. H. Xia, M. Lai, and L. Lu, *Journal of Materials Chemistry*, **20**, 6896 (2010).
26. Y. Sun, X. Hu, W. Luo, F. Xia, and Y. Huang, *Advanced Functional Materials*, **23**, 2436 (2013).
27. R.-C. Lee, Y.-P. Lin, Y.-T. Weng, H.-A. Pan, J.-F. Lee, and N.-L. Wu, *Journal of Power Sources*, **253**, 373 (2014).
28. M. Gaberscek, R. Dominko, and J. Jamnik, *Electrochemistry Communications*, **9**, 2778 (2007).
29. S.-B. Yoon, K. C. Roh, and K.-B. Kim, *Journal of The Electrochemical Society*, **161**, H365 (2014).
30. S.-B. Ma, K.-Y. Ahn, E.-S. Lee, K.-H. Oh, and K.-B. Kim, *Carbon*, **45**, 375 (2007).
31. V. Etacheri, O. Haik, Y. Goffer, G. A. Roberts, I. C. Stefan, R. Fasching, and D. Aurbach, *Langmuir*, **28**, 965 (2012).
32. V. G. Makhankova, O. V. Khavryuchenko, V. V. Lisnyak, and V. N. Kokozay, Preparation of binary M/Mn (M = Co, Cu, Zn) oxide catalysts by thermal degradation of heterobimetallic complexes, in: M. D. S. H. P. A. J. J. A. M. E. M. Gaigneaux and P. Ruiz (Eds.) *Studies in Surface Science and Catalysis*, Elsevier, 2010, pp. 563.
33. X. Wang and H. Dai, *Nat Chem*, **2**, 661 (2010).
34. C. W. Na, S.-Y. Park, J.-H. Chung, and J.-H. Lee, *ACS Applied Materials & Interfaces*, **4**, 6565 (2012).
35. M. Ahmad, S. Yingying, A. Nisar, H. Sun, W. Shen, M. Wei, and J. Zhu, *Journal of Materials Chemistry*, **21**, 7723 (2011).
36. S.-B. Yoon, H.-K. Kim, K. C. Roh, and K.-B. Kim, *Journal of The Electrochemical Society*, **162**, A667 (2015).
37. S.-B. Yoon, H.-K. Song, K. C. Roh, and K.-B. Kim, *Journal of The Electrochemical Society*, **161**, A137 (2014).